14. Boyer, P. & Kasevich, M. A. Heisenberg-limited spectroscopy with degenerate Bose-Einstein gases. *Phys. Rev. A* **56,** R1083–R1086 (1997).
15. Santarelli, G. *et al.* Quantum projection noise in an atomic fountain: A high stability cesium frequency standard. *Phys. Rev. Lett.* **82,** 4619–4622 (1999).
16. Sørensen, A. & Mølmer, K. Spin-spin interaction and spin squeezing in an optical lattice. *Phys. Rev. Lett.* **83,** 2274–2277 (1999).
17. Hald, J., Sørensen, J. L., Schori, C. & Polzik, E. S. Spin squeezed atoms: A macroscopic entangled ensemble created by light. *Phys. Rev. Lett.* **83,** 1319–1322 (1999).
18. Kuzmich, A., Mandel, L. & Bigelow, N. P. Generation of spin squeezing via continuous quantum nondemolition measurement. *Phys. Rev. Lett.* **85,** 1594–1597 (2000).
19. Mølmer, K. & Sørensen, A. Multiparticle entanglement of hot trapped ions. *Phys. Rev. Lett.* **82,** 1835–1838 (1999).
20. Bollinger, J. J., Itano, W. M., Wineland, D. J. & Heinzen, D. J. Optimal frequency measurements with maximally correlated states. *Phys. Rev. A* **54,** 4649–4652 (1996).

Acknowledgements

This work was supported by the Austrian Science Foundation, the European Union project EQUIP, the TMR European network, the ESF under the PESC program "Quantum Information", the Institute for Quantum Information GmbH, and the Thomas B. Thriges Center for Kvanteinformatik. A.S. acknowledges the hospitality of the University of Innsbruck.

Correspondence and requests for materials should be addressed to A.S. (e-mail: anderss@ifa.au.dk).

Indium phosphide nanowires as building blocks for nanoscale electronic and optoelectronic devices

Xiangfeng Duan*†, Yu Huang*†, Yi Cui*, Jianfang Wang* & Charles M. Lieber*‡

** Department of Chemistry and Chemical Biology, ‡ Division of Engineering and Applied Sciences, Harvard University, Cambridge, Massachusetts 02138, USA*
† These authors contributed equally to this work

Nanowires and nanotubes carry charge and excitons efficiently, and are therefore potentially ideal building blocks for nanoscale electronics and optoelectronics[1,2]. Carbon nanotubes have already been exploited in devices such as field-effect[3,4] and single-electron[5,6] transistors, but the practical utility of nanotube components for building electronic circuits is limited, as it is not yet possible to selectively grow semiconducting or metallic nanotubes[7,8]. Here we report the assembly of functional nanoscale devices from indium phosphide nanowires, the electrical properties of which are controlled by selective doping. Gate-voltage-dependent transport measurements demonstrate that the nanowires can be predictably synthesized as either n- or p-type. These doped nanowires function as nanoscale field-effect transistors, and can be assembled into crossed-wire p–n junctions that exhibit rectifying behaviour. Significantly, the p–n junctions emit light strongly and are perhaps the smallest light-emitting diodes that have yet been made. Finally, we show that electric-field-directed assembly can be used to create highly integrated device arrays from nanowire building blocks.

We prepared single-crystal InP nanowires with n- and p-type doping by laser-assisted catalytic growth (LCG)[9,10]. Field-emission scanning electron microscopy (FE-SEM) images of the doped nanowires (Fig. 1a) show that the wires are up to tens of micrometres long, with diameters of the order of 10 nm. High-resolution transmission electron microscopy (TEM) images (Fig. 1a inset) show that the doped nanowires are single crystals with ⟨111⟩ growth directions. To confirm the presence and type of dopants in the nanowires, we have performed gate-dependent, two-terminal transport measurements on individual wires, as the conductance will respond in an opposite way to changes in gate voltage (V_g) for n-and p-type nanowires: $V_g > 0$ will lead to an accumulation of electrons and increase in conductance for the former, but will deplete holes and reduce conductance for the latter[11]. Figures 1b and c show the typical gate-dependent current–voltage (I–V) curves obtained from individual Te- and Zn-doped nanowires, respectively. These curves are linear or nearly linear at $V_g = 0$, indicating that the metal electrodes make ohmic contact to the nanowires. This ohmic nature was substantiated by conductance and four-terminal measurements (see Supplementary Information). The transport data recorded on Te-doped nanowires (Fig. 1b) show an increase in conductance for $V_g > 0$, while the conductance decreases for $V_g < 0$. These data clearly show that Te-doped InP nanowires are n-type. Gate-dependent transport data recorded on Zn-doped nanowires show

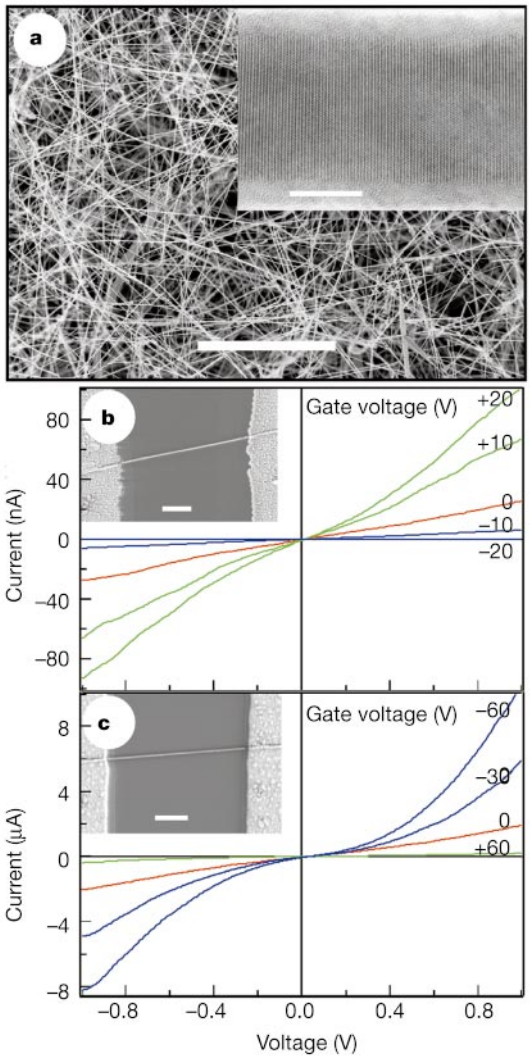

Figure 1 Doping and electrical transport of InP nanowires. **a**, A typical FE-SEM image of Zn-doped InP nanowires. Scale bar, 10 μm. Inset, lattice resolved TEM image of one 26-nm-diameter NW. The (111) lattice planes are visible perpendicular to the wire axis. Scale bar, 10 nm. The TEM studies show that nanowires are typically coated with a 1–2-nm amorphous overlayer. This thin layer is attributed to oxides formed when the nanowires are exposed to air after synthesis. The overall composition of individual nanowires determined by energy dispersive X-ray analysis was found to be 1:1 In:P, thus confirming their stoichiometric composition. **b** and **c**, Gate-dependent I–V behaviour for Te- and Zn-doped NWs, respectively. Insets show the nanowire measured with two-terminal Ni/In/Au contact electrodes. Scale bars, 1 μm. The diameter of the nanowire in **b** is 47 nm, while that in **c** is 45 nm. Gate voltages used in the measurements are indicated on the corresponding I–V curves (right side). Data were recorded at room temperature.

opposite changes in conductance with variation in V_g: for $V_g > 0$, conductance decreases and for $V_g < 0$ conductance increases (Fig. 1c). Zn-doped InP nanowires are therefore p-type.

Our results are reproducible. Measurements made on more than 20 individual nanowires of each dopant type show gate effects in each case that are consistent with the dopant used during synthesis. In addition, V_g can be used to completely deplete electrons and holes in n- and p-type nanowires such that the conductance becomes immeasurably small. For example, the conductance of the nanowire in Fig. 1b can be switched from a conducting (on) to an insulating (off) state when $V_g \leq -20$ V; thus it functions as a field-effect transistor (FET). Conductance modulations as large as 4–5 orders of magnitude have been observed. The relatively large switching voltage is related to the thick (600 nm) oxide dielectric used in our measurements. This gate-dependent behaviour is similar to that of metal-oxide-semiconductor (MOS) FETs[12] and recent semiconducting nanotube FETs[3,4]. An important distinction of our work with respect to nanotubes is that predictable semiconducting behaviour can be achieved in every nanowire. Because these InP nanowires are produced in bulk quantities, they represent a readily available material for assembling devices and device arrays.

The availability of well-defined n- and p-type nanowire building blocks opens up the possibility of creating complex functional devices by forming junctions between two or more such wires. To explore this opportunity, we have investigated n–n, p–p and p–n junctions formed by crossing two n-type, two p-type, and one n-type and one p-type nanowire, respectively. Significantly, the types of junctions studied are controllable for every experiment as we can select the types of nanowires used to produce the crossed junction before assembly. Figure 2a shows a representative crossed nanowire device formed from one of 29 nm diameter and one of 40 nm diameter.

Figures 2b and c show I–V data recorded on n–n and p–p junctions, respectively. The transport data recorded on the individual nanowires (AC, BD) show linear or nearly linear I–V behaviour (green and blue curves in Fig. 2b and c respectively). As discussed above, these results show that the metal electrodes make ohmic or nearly ohmic contact to the nanowires, and hence will not make significant contributions to the I–V measurements across junctions. In general, transport measurements made across the n–n and p–p junctions also show linear or nearly linear behaviour, and allow us to infer two important points about crossed nanowire junctions. First, interface oxide between individual nanowires does not produce a significant tunnelling barrier, as such a barrier would lead to highly nonlinear I–V curves. Second, the I–V curves recorded through each pair (AB, AD, CB, CD in Fig. 2) of adjacent arms are similar and $I(V)$ is smaller than through individual nanowires. These results demonstrate that the junction dominates the transport behaviour. Overall, our data indicate that crossed nanowires make reasonably good electrical contact with each other, despite the small contact area (10^{-12}–10^{-10} cm^2) and simple method of junction fabrication.

The good contact between crossed nanowires suggests that functional devices should be possible, and thus we have explored p–n junctions made from crossed p- and n-type nanowires. These junctions can be made reproducibly by sequential deposition of dilute solutions of n- and p-type nanowires with intermediate drying. Typical I–V data recorded on a crossed p–n junction (Fig. 2d) shows linear or nearly linear I–V for the individual n- and p-type nanowire components (green and blue curves), which indicates that they are ohmically contacted, and current rectification across the p–n junction (red curves); that is, little current flows in reverse bias, whereas there is a sharp current onset in forward bias. This diode-like behaviour is similar to bulk semiconductor p–n junctions, which form the basis for many critical electronic and

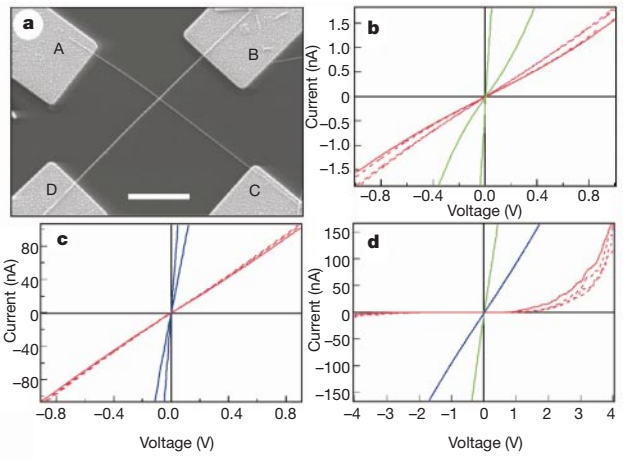

Figure 2 Crossed nanowire junctions and electrical properties. **a**, FE-SEM image of a typical crossed nanowire device with Ni/In/Au contact electrodes. The four arms are designated as A, B, C, D for simplicity of discussion. Scale bar, 2 μm. The diameters of the nanowires are 29 nm (AC) and 40 nm (BD); the diameters of the nanowires used to make devices were in the range of 20–75 nm. **b–d**, I–V behaviour of n–n, p–p and p–n junctions, respectively. The green and blue curves correspond respectively to the I–V behaviour of individual n- and p-type nanowires in the junctions. The red curves represent the I–V behaviour across the junctions. The current recorded for the p- and n-type nanowires in **d** has been divided by 10 for better viewing. Solid lines, transport behaviour across one pair of adjacent arms; dashed lines, transport behaviour across the other three pairs of adjacent arms. Data were recorded at room temperature.

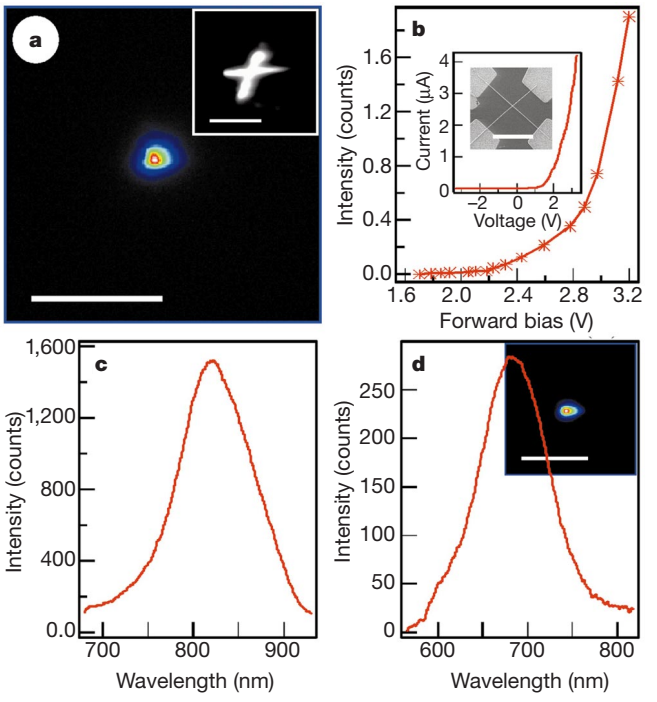

Figure 3 Optoelectrical characterization of nanowire p–n junctions. **a**, Electroluminescence (EL) image of the light emitted from a forward-biased nanowire p–n junction at 2.5 V. Inset, photoluminescence (PL) image of the junction. Scale bars, 5 μm. **b,** EL intensity versus voltage. Inset, I–V characteristics; inset in this inset, FE-SEM image of the junction itself. Scale bar, 5 μm. The n-type and p-type nanowires forming this junction have diameters of 65 and 68 nm, respectively. **c,** EL spectrum of the junction shown in **a**. The spectrum peaks at 820 nm. **d,** EL spectrum recorded from a second forward-biased crossed nanowire p–n junction. The EL maximum occurs at 680 nm. Inset, EL image showing that the EL originates from the junction region. Scale bar, 5 μm. The n-type and p-type nanowires forming this junction have diameters of 39 and 49 nm, respectively. The colours in **a** and the inset to **d** correspond to EL intensity, with black equal to zero counts and white equal to the highest counts.

optoelectronic devices. In a standard p–n junction, rectification arises from the potential barrier formed at the interface between p- and n-type materials[12]. In the case of our nanowires, this picture may be modified, owing to a thin oxide at the interface (see Supplementary Information). When either type of junction is forward biased, the barrier is reduced and a relatively large current can flow through the junction; on the other hand, only a small current can flow in reverse bias as the barrier is further increased.

There are several reasons why the observed rectification can be attributed to the p–n junction formed between the crossed p- and n-type InP nanowires. First, the linear or nearly linear *I*–*V* behaviour of individual p- and n-type nanowires used to make the junction shows that ohmic contacts have been made between them and metal electrodes. This excludes rectification arising from metal–semiconductor Schottky diodes[12]. Second, the *I*–*V* behaviour of the junction determined through every pair (AB, AD, BC, CD) of adjacent electrodes (red curves in Fig. 2d) exhibits a similar rectification effect and current level, which is also much smaller than the current level through the individual nanowires. These results demonstrate that the junction dominates the *I*–*V* behaviour. Third, four-terminal measurements in which current is passed through two adjacent electrodes (for example, AB), while the junction voltage drop is measured across two independent electrodes (for example, CD), exhibit similar *I*–*V* curves with only a slightly smaller voltage drop (0.1–0.2 V) compared to the two-terminal case (see Supplementary Information). Last, measurements made on 10 independent p–n junctions showed similar rectification in the *I*–*V* data; that is, significant current can only flow through p–n junctions when the p-type nanowire is positively biased.

The above data show unambiguously that we can rationally assemble nanoscale p–n junctions. In direct-bandgap semiconductors like InP, the p–n junction forms the basis for optoelectronics devices, including light-emitting diodes (LED) and lasers. To assess such functions in our nanoscale devices, we have studied the photoluminescence (PL) and electroluminescence (EL) from crossed nanowire p–n junctions. Significantly, EL can be readily observed from these nanoscale p–n junctions in forward bias (Fig. 3a). A PL image of a crossed nanowire junction (inset) shows two crossed wire-like structures, and comparison of the EL and PL images shows that the position of the EL maximum corresponds to the crossing point in the PL image, thus demonstrating that the light originates from the nanowire p–n junction.

The *I*–*V* characteristics of the junction (Fig. 3b inset) shows clear rectification with a sharp current onset at ~1.5 V. The curve of EL intensity versus voltage shows (Fig. 3b) that significant light can be detected with our system at a voltage as low as 1.7 V. The EL intensity increases rapidly with bias voltage, and resembles the *I*–*V* behaviour. The EL spectrum (Fig. 3c) shows a maximum intensity around 820 nm, which is substantially blue-shifted relative to the bulk bandgap of InP (925 nm). EL results recorded from a p–n junction assembled using smaller diameter nanowires (Fig. 3d) showed a larger blue-shift, and thus suggest that these shifts may be due in part to quantum confinement[13] of the excitons, although other factors also contribute (M.S. Gudiksen, J.W., X.D. and C.M.L., unpublished results). The quantum efficiency (electron to photon) of these initial devices is relatively low, ~0.001%, which is not surprising as we have paid little attention to optimization. The efficiency is actually comparable to that (~0.002%) of early bulk InP LEDs[14]. We attribute the low quantum efficiency to non-radiative recombination via surface states, and believe that this deleterious process can be reduced by surface passivation[15,16].

Development of highly integrated devices based on nanowires will require techniques to align and assemble these building blocks into well-defined arrays. To demonstrate this next level of complexity, we have exploited electric fields to align and position individual nanowires into parallel and crossed arrays (Fig. 4a). A similar approach has been discussed[17] elsewhere. The potential of this approach was first demonstrated by aligning many nanowires between parallel electrodes (Fig. 4b). FE-SEM images show that nearly all of the wires are aligned perpendicular to the parallel electrodes and along the direction of the electric field. Such electric-field assembly of nanowires between an array of electrodes (Fig. 4c) shows that individual wires can be positioned to bridge pairs of diametrically opposed electrodes and form a parallel array. In addition, by changing the field direction, the alignment can be done in a layer-by-layer fashion to produce crossed nanowire junctions (Fig. 4d). These data show that electric-field assembly represents a viable strategy for organizing individual nanowires with good directional and spatial control. We believe that highly integrated functional devices would be readily accessible using our nanowire building blocks in conjunction with this electric-field and/or other assembly techniques[18].

Taken as a whole, the results presented here provide a rational approach for the bottom-up assembly of nanoscale electronic and optoelectronic devices. The demonstrated ability to assemble active devices in the absence of multi-billion-dollar fabrication lines is critically important to the field, and we believe that it augurs well for immediate and longer-term advances. We believe that the broad range of nanowire materials now available[10] and the clearly defined ability to control their electronic properties will make possible nanoscale LEDs that cover the entire visible and near-infrared range (for example, GaN nanowires for blue colours[19]). Nanoscale light sources might be useful in creating new types of highly parallel sensors and for optical interconnects in nanoelectronics. We consider that the assembly of doped nanowire building blocks has great potential for creating many other types of electronic devices—and possibly even lasers. □

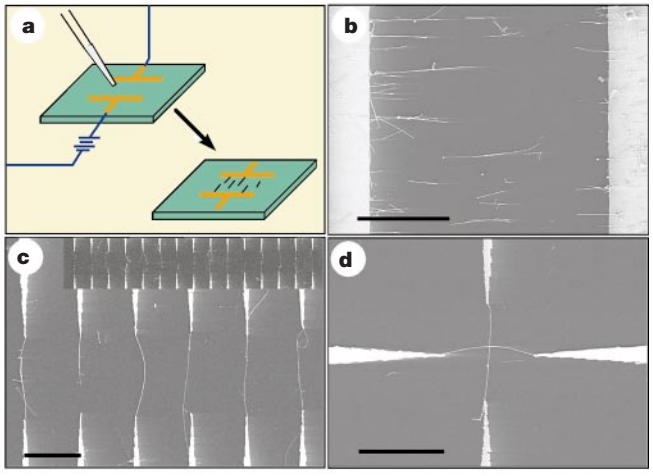

Figure 4 Parallel and orthogonal assembly of nanowires with electric fields. **a,** Schematic view of alignment by electric field. The electrodes (shown orange) are biased at 50–100 V after a drop of nanowire solution is deposited on the substrate (blue). **b,** Parallel array of nanowires aligned between two parallel electrodes. The nanowires were suspended in chlorobenzene and aligned using an applied bias of 100 V. **c**, Spatially positioned parallel array of nanowires obtained following electric-field assembly using a bias of 80 V. Inset, 15 pairs of parallel electrodes with individual nanowires bridging each diametrically opposed electrode pair. **d,** Crossed nanowire junction obtained using layer-by-layer alignment with the electric field applied in orthogonal directions in the two assembly steps. The applied bias in both steps was 80 V. Scale bars in **b–d**, 10 μm.

Methods

Nanowire synthesis and characterization

InP nanowires (NWs) were synthesized using LCG[9,10]. The LCG target typically consisted of 94% (atomic ratio) InP, 5% Au as the catalyst, and 1% of Te or Zn as the doping element.

The furnace temperature (middle) was set at 800 °C during growth, and the target was placed at the upstream end rather than middle of the furnace. A pulsed (8-ns, 10-Hz) Nd-YAG laser (wavelength 1,064 nm) was used to vaporize the target. Typically, growth was performed for 10 min with NWs collected at the downstream, cool end of the furnace.

Electrical characterization

Transport measurement on individual NWs were carried out using published procedures[11]. NWs were first dispersed in ethanol, and then deposited onto oxidized silicon substrates (600 nm oxide, 1–10 Ω cm resistivity), with the conductive silicon used as a back gate. Electrical contact to the NWs was defined using electron beam lithography (JEOL 6400). Ni/In/Au contact electrodes were thermally evaporated. Electrical transport measurements were made using a home-built system with <1 pA noise under computer control.

Junctions (n–n and p–p) were obtained by random deposition. We first deposited NWs onto oxidized silicon substrates using relatively high concentrations, determined the positions of crossed NWs, and then defined electrodes on all four arms of the cross by electron beam lithography. Ni/In/Au electrodes were used to make contact to the NWs.

p–n junctions were obtained by layer-by-layer deposition. First, a dilute solution of one type (for example, n-type) of NW was deposited on the substrate, and the positions of individual NWs were recorded. In a second step, a dilute solution of the other type (for example, p-type) of NW was deposited, and the positions of crossed n- and p-type NWs were recorded. Metal electrodes were then defined and transport behaviour was measured.

Optoelectrical characterization

EL was studied with a home-built micro-luminescence instrument[20]. PL or scattered light (514 nm, Ar-ion laser) was used to locate the position of the junction. When the junction was located, the excitation laser was shut off, and then the junction was forward biased. EL images were taken with a liquid-nitrogen-cooled CCD camera, and EL spectra were obtained by dispersing EL with a 150 lines mm^{-1} grating in a 300-mm spectrometer.

Received 11 July; accepted 25 October 2000.

1. Hu, J., Odom, T. W. & Lieber, C. M. Chemistry and physics in one dimension: synthesis and properties of nanowires and nanotubes. *Acc. Chem. Res.* **32,** 435–445 (1999).
2. Dekker, C. Carbon nanotubes as molecular quantum wires. *Phys. Today* **52**(5), 22–28 (1999).
3. Tans, S. J., Verschueren, R. M. & Dekker, C. Room temperature transistor based on a single carbon nanotube. *Nature* **393,** 49–52 (1998).
4. Martel, R., Schmidt, T., Shea, H. R., Hertel, T. & Avouris, P. Single- and multi-wall carbon nanotube field effect transistors. *Appl. Phys. Lett.* **73,** 2447–2449 (1998).
5. Tans, S. J. *et al.* Individual single-wall carbon nanotubes as quantum wires. *Nature* **386,** 474–477 (1997).
6. Bockrath, M. *et al.* Single electron transport in ropes of carbon nanotubes. *Science* **275,** 1922–1925 (1997).
7. Odom, T. W., Huang, J.-L., Kim, P. & Lieber, C. M. Atomic structure and electronic properties of single-walled carbon nanotubes. *Nature* **391,** 62–64 (1998).
8. Wildoer, J. W. G., Venema, L. C., Rinzler, A. G., Smalley, R. E. & Dekker, C. Electronic structure of atomically resolved carbon nanotubes. *Nature* **391,** 59–62 (1998).
9. Morales, A. M. & Lieber, C. M. A laser ablation method for the synthesis of crystalline semiconductor nanowires. *Science* **279,** 208–211 (1998).
10. Duan, X. & Lieber, C. M. General synthesis of compound semiconductor nanowires. *Adv. Mater.* **12,** 298–302 (2000).
11. Cui, Y., Duan, X., Hu, J. & Lieber, C. M. Doping and electrical transport in silicon nanowires. *J. Phys. Chem. B* **104,** 5213–5216 (2000).
12. Sze, S. M. *Physics of Semiconductor Devices* (Wiley, New York, 1981).
13. Alivisatos, A. P. Semiconductor clusters, nanocrystal, and quantum dots. *Science* **271,** 933–937 (1996).
14. Bolm, G. M. & Woodall, J. M. Efficient electroluminescence from InP diodes grown by liquid-phase epitaxy. *Appl. Phys. Lett.* **17,** 373–376 (1970).
15. Bessolov, V. N. & Lebedev, M. V. Chalcogenide passivation of III-V semiconductor surfaces. *Semiconductors* **32,** 1141–1156 (1998).
16. Micic, O. I., Sprague, J., Lu, Z. & Nozik, A. J. Highly efficient band edge emission from InP quantum dots. *Appl. Phys. Lett.* **68,** 3150–3152 (1996).
17. Smith, P. A. Electric-field assisted assembly and alignment of metallic nanowires. *Appl. Phys. Lett.* **77,** 1399–1401 (2000).
18. Xia, Y. N., Rogers, J. A., Paul K. E. & Whitesides, G. M. Unconventional methods for fabricating and patterning nanostructures. *Chem. Rev.* **99,** 1823–1848 (1999).
19. Duan, X. & Lieber, C. M. Laser assisted catalytic growth of single crystal GaN nanowires. *J. Am. Chem. Soc.* **122,** 188–189 (2000).
20. Duan, X., Wang, J. & Lieber, C. M. Synthesis and optical properties of GaAs nanowires. *Appl. Phys. Lett.* **76,** 1116–1168 (2000).

Supplementary information is available on *Nature*'s World-Wide Web site (http://www.nature.com) or as paper copy from the London editorial office of *Nature*.

Acknowledgements

We thank H. Park, M.S. Gudiksen, J.-L. Huang, K. Kim, T. Oosterkamp & S.-I. Yang for discussions. This work was supported by the US Office of Naval Research, Defense Advanced Projects Research Agency, and the National Science Foundation.

Correspondence and requests for materials should be addressed to C.M.L. (e-mail: cml@cmliris.harvard.edu).

Computational design of direct-bandgap semiconductors that lattice-match silicon

Peihong Zhang*, Vincent H. Crespi*, Eric Chang†, Steven G. Louie† & Marvin L. Cohen†

** Department of Physics, The Pennsylvania State University, 104 Davey Lab, University Park, Pennsylvania 16802-6300, USA*
† Department of Physics, University of California at Berkeley, Berkeley, California 94720 and Materials Sciences Division, Lawrence Berkeley Laboratory, Berkeley, California 94720, USA

Crystalline silicon is an indirect-bandgap semiconductor, making it an inefficient emitter of light. The successful integration of silicon-based electronics with optical components will therefore require optically active (for example, direct-bandgap) materials that can be grown on silicon with high-quality interfaces. For well ordered materials, this effectively translates into the requirement that such materials lattice-match silicon: lattice mismatch generally causes cracks and poor interface properties once the mismatched overlayer exceeds a very thin critical thickness. But no direct-bandgap semiconductor has yet been produced that can lattice-match silicon, and previously suggested structures[1] pose formidable challenges for synthesis. Much recent work has therefore focused on introducing compliant transition layers between the mismatched components[2–4]. Here we propose a more direct solution to integrating silicon electronics with optical components. We have computationally designed two hypothetical direct-bandgap semiconductor alloys, the synthesis of which should be possible through the deposition of specific group-IV precursor molecules[5,6] and which lattice-match silicon to 0.5–1% along lattice planes with low Miller indices. The calculated bandgaps (and hence the frequency of emitted light) lie in the window of minimal absorption in current optical fibres.

Bulk silicon is an indirect-bandgap semiconductor, that is the lowest-energy transition from valence to conduction bands involves a change in crystal momentum. Such materials are typically not suitable for optical applications since nonradiative events dominate the interband transitions. However, silicon is nearly surrounded by direct-bandgap elemental (unary) and compound semiconductors in the periodic table. Moving downwards from Si, the unary group-IV materials acquire larger cores containing *d* electrons; these states affect the conduction band states through orthogonality requirements and changes in the overall volume. On moving from silicon to germanium to tin, the $\Gamma_{2'}$ conduction band (as labelled in silicon) at $k = 0$ drops in energy until, in grey tin, the material acquires a direct (and vanishing) bandgap at $k = 0$. Moving across the periodic table, GaAs, a prototypical direct-bandgap semiconductor, differs from Si or Ge in that the constituents have different electronegativities. The resulting antisymmetric component in the crystal potential flattens the bands and opens the bandgap. In addition, the Γ_6 point of the conduction band drops relative to the other points in the band until it becomes the bottom of the conduction band in most of the well-known direct-bandgap group III–V and II–VI semiconductors.

These well-known results suggest that perhaps one can combine these mechanisms: larger cores and partial ionicity, within alloys containing only group-IV elements wherein the difference in rows of the periodic table provides the contrast in electronegativity. Such a system is likely to require the presence of tin to obtain a direct bandgap[7–10]; the combination of tin (which is substantially larger than silicon) with carbon (which is substantially smaller than silicon) not only affords the greatest contrast in electronegativity